Ab initio calculations of the optical properties of 4-Å-diameter single-walled nanotubes

M. Machón, S. Reich, and C. Thomsen
Institut für Festkörperphysik, Technische Universität Berlin, Hardenbergstrasse 36, 10623 Berlin, Germany

D. Sánchez-Portal
Centro Mixto CSIC-UPV/EHU and Donostia International Physics Center (DIPC), Apartado 1072, 20080 San Sebastián, Spain

P. Ordejón
Institut de Ciència de Materials de Barcelona (CSIC), Campus de la Universitat Autònoma de Barcelona, E-08193 Bellaterra, Barcelona, Spain

(Received 26 March 2002; revised manuscript received 31 May 2002; published 8 October 2002)

We performed density-functional theory calculations in the local-density approximation of the structural, electronic, and optical properties of 4-Å-diameter single-walled carbon nanotubes. The calculated relaxed geometries show significant deviations from the ideal rolled graphene sheet configuration. We study the effect of the geometry on the electronic band structure finding the metallic character of the (5,0) nanotube to be a consequence of the high curvature of the nanotube wall. Calculations of the dielectric function and optical absorption of the isolated nanotubes were performed under light polarized parallel and perpendicular to the tube axis. We compare our results to measurements of the optical absorption of zeolite-grown nanotubes and are able to assign the observed maxima to the nanotube chiralities.

DOI: 10.1103/PhysRevB.66.155410 PACS number(s): 78.67.Ch, 73.63.Fg, 78.40.Ri

Carbon nanotubes, due to their intrinsic one-dimensional properties and their promising applications have attracted the attention of many theoretical and experimental research groups. The specific comparison of theory and experiment is difficult because of the wide range of diameters and chiralities usually present in the samples. Nanotubes having very similar structures can have radically different properties and require independent calculations. Single-walled carbon nanotubes (SWNT's) grown within the channels of a zeolite[1] present several advantages in this respect. First, the nanotubes arranged in the channels of this material are forced to have a narrow diameter distribution around 4 Å, reducing the possible nanotube chiralities to three: (3,3), (5,0), and (4,2). Furthermore, the small unit cell of these nanotubes allows the calculation of their properties using *ab initio* methods. The second advantage is the alignment of the nanotubes in the zeolite channels, which makes possible a study, e.g., of selection rules.

In this paper, we present first-principles calculations of the structural, electronic, and optical properties of 4-Å-diameter SWNT's. We discuss the relaxed geometry of the (3,3), (5,0), and (4,2) nanotubes comparing it to the ideal cylindrical configuration and its effect on the band structure. The effect of the strong curvature of the nanotube wall is studied more closely, comparing the zone folding of the *ab initio* results of graphene with *ab initio* calculations of the band structure. The response of the nanotubes to light polarized both parallel and perpendicular with respect to the nanotube axis is studied and found to be strongly anisotropic. We compare our results to optical-absorption measurements of zeolite-grown SWNT's obtaining excellent agreement.[1]

Ab initio calculations for the (3,3), (5,0), and (4,2) nanotubes were performed using the SIESTA code[2,3] within the local-density approximation as parametrized by Perdew and Zunger.[4] The core electrons were replaced by nonlocal norm-conserving pseudopotentials.[5] A double-ζ, singly polarized (DZP) basis set of localized atomic orbitals plus a diffuse 3*s* orbital were used for the valence electrons. The inclusion of the 3*s* shell is instrumental for the description of the electronic spectrum above 3 eV. More precisely, the DZP basis, without the inclusion of the 3*s* orbital, fails to reproduce the position of the dispersive band appearing 3 eV above the Fermi level at the Γ point in the case of the band structure of graphene (see Fig. 1), placing it at higher energies. A cutoff radius of 10 a.u. was used for the 3*s* shell. For the DZP basis, cutoff radii of 5.12 a.u. for the *s* and 6.25 a.u. for the *p* and *d* orbitals were used, as determined from an energy shift of 50 meV by localization,[6,7] which was chosen as the one that minimizes the total energy for a graphene sheet. Increasing the cutoff of the orbitals only changes the *total* energies of the nanotubes considered here by less than 0.1 eV/atom, and has virtually no effect on the structure and the

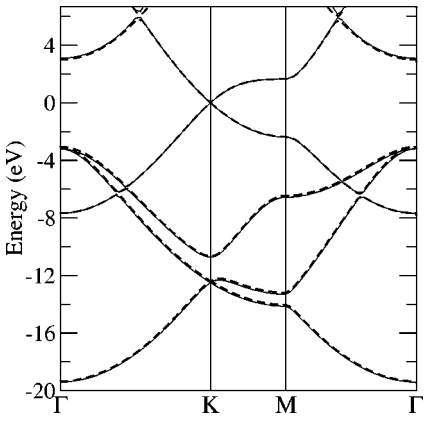

FIG. 1. Comparison of the band structure of graphene obtained with a DZP basis set of localized orbitals plus diffuse 3*s* functions (full lines) and with plane waves (dashed lines).

TABLE I. Geometry parameters for the ideal rolled graphene sheet and for the relaxed configuration. The parameters are defined as in Fig. 2.

		Radius	Lattice Constant	a	b	c	α	β	γ
(3,3)	Relaxed	2.10	2.47	1.433	1.438		116.2	118.7	
	Cylinder	2.041	2.468	1.423	1.396		115.6	120.3	
(5,0)	Relaxed	2.035	4.27	1.412	1.450		119.8	111.2	
	Cylinder	1.96	4.28	1.425	1.407		120.4	110.2	
(4,2)	Relaxed	2.14	11.28	1.440	1.421	1.443	114.1	118.7	118.7
	Cylinder	2.079	11.31	1.399	1.425	1.420	113.3	120.4	118.1

energies of the electronic states. In order to demonstrate the accuracy of the basis set used here, we compare in Fig. 1 the calculated band structure of a graphene sheet, with the results computed using a 50-Ry plane-wave expansion and the same pseudopotentital and exchange functional, obtaining an excellent agreement up to at least 6.5 eV.

In order to avoid interaction between the images, a unit cell with a length of 11 Å in the x and y directions was used. Integrations in k space were performed over 16 k points for the (3,3) and (5,0) nanotubes, and three k points for the (4,2) nanotube in the k_z direction. Real-space integrations were done in a grid with a cutoff $\approx$270 Ry for the (3,3) and (5,0) nanotubes and 250 Ry for the (4,2) nanotube.

The atomic positions were relaxed by a conjugate gradient minimization until the forces on the atoms were less than 0.04 eV/Å. For the relaxed structure we calculated the theoretical lattice constant. In Table I the results of the relaxation are shown together with the parameters corresponding to the ideal cylindrical geometry obtained by rolling up the graphene plane.[8] The bond lengths and angles for the ideal configuration depend on the chirality, due to the curvature of the nanotube wall. We used the calculated lattice constant of graphene $a=2.468$ Å. The lattice constant of the nanotubes in z direction changed by less than 0.3% during the relaxation. The calculated average radii are $\approx$3% larger for the relaxed geometry in agreement with the trend indicated by Sánchez-Portal *et al.*[9] This change in radius corresponds to different changes of the bond lengths and angles depending on the particular geometry of the tube. The bonds having smallest angles with the tube axis are changed the least with respect to the ideal structure, as expected [bond a for the (3,3) and (5,0) nanotubes, b and c for the (4,2) tube]. The bonds in the direction of the circumference are more affected by the curvature and experience changes up to 3%. The angles change less than 1.5% for the three nanotubes.

The electronic band structures were calculated using the relaxed geometries obtained above. The results, shown in Fig. 3, are essentially the same as those obtained by Li *et al.*[1]

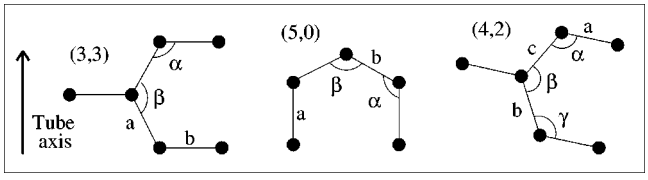

FIG. 2. Geometry parameters of the 4-Å-diameter nanotubes.

using an independent plane-wave method. The most remarkable feature is the metallic character of the (5,0) SWNT, which is expected to be semiconducting in the zone folding approximation. Blase *et al.*[10] showed, for zigzag nanotubes as small as (6,0), how the increasing curvature of the graphene sheet can enforce a rehybridization of the π and σ orbitals of carbon atoms, which is not present in the planar structure. The effect of curvature, neglected in the zone folding approach, becomes essential in the case of the 4-Å nanotubes as can be seen in Fig. 4. The solid lines show *ab initio* zone folding calculated bands, in which the curvature is completely neglected, while the dotted lines show again the *ab initio* calulation for the relaxed geometry. It is clearly seen how the curvature shifts down the π^* derived nanotube bands, which in the case of the (5,0) nanotube leads to the metallic character. The (4,2) nanotube is semiconducting as expected, but with a 0.2-eV indirect gap, instead of the 2-eV direct gap obtained from zone folding. For these small tubes the valence bands are not well reproduced by the zone folding approach, contrary to the observation for nanotubes with larger radii.[11] Furthermore, the valence and conduction bands of the three tubes are strongly asymmetric with respect to the Fermi level in contrast to the nearest-neighbor tight-binding approach in which only the π and π^* orbitals are taken into account.

We also calculated the band structure of the 4-Å-diameter

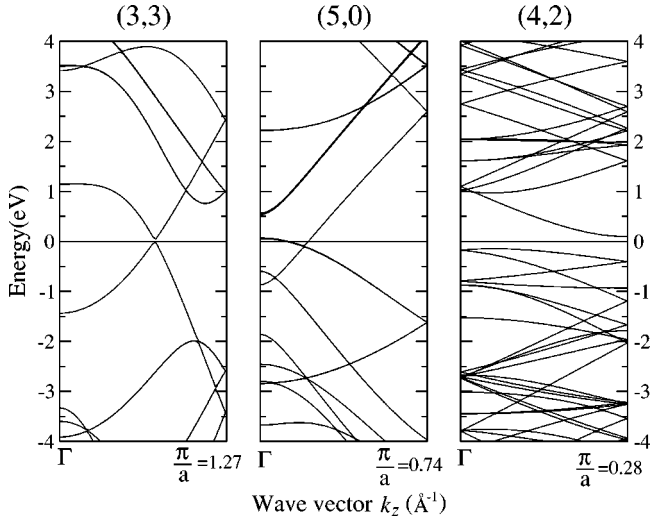

FIG. 3. Calculated electronic band structures of the relaxed 4-Å SWNT's. The Fermi level is at 0 eV.

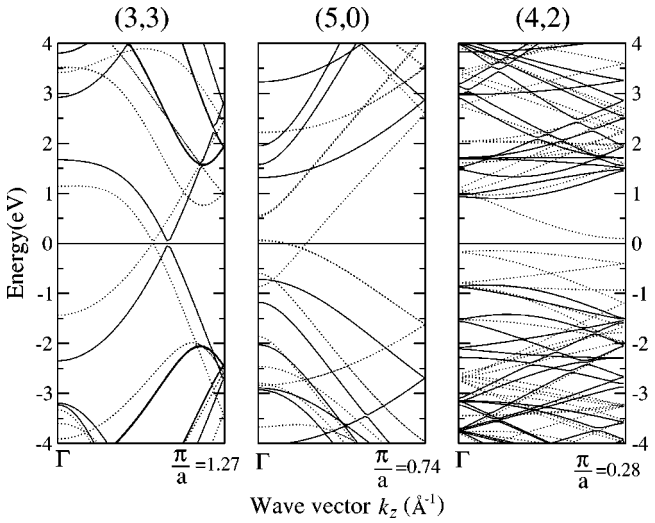

FIG. 4. Solid line represents zone folding electronic band structures of the 4-Å SWNT's. Dotted line represents *ab initio* electronic band structures of the relaxed 4-Å nanotubes. The Fermi level is at 0 eV.

nanotubes in the ideal cylindrical configuration obtained from rolling a graphene sheet, as can be seen in Fig. 5. The changes depend strongly on the chirality and the specific band, and can be as large as ≈ 1 eV. Nevertheless, the differences shown in Fig. 5 are much smaller than the ones coming from the curvature, especially in the region around the Fermi energy (compare Fig. 4). In particular, it should be noted that the metallic character of the (5,0) nanotube is already obtained for the cylindrical geometry and thus not an effect of the structural relaxation.

The optical response of the SWNT's was obtained using first-order time-dependent perturbation theory to calculate the dipolar transition matrix elements between occupied and unoccupied single-electron eigenstates, as implemented in

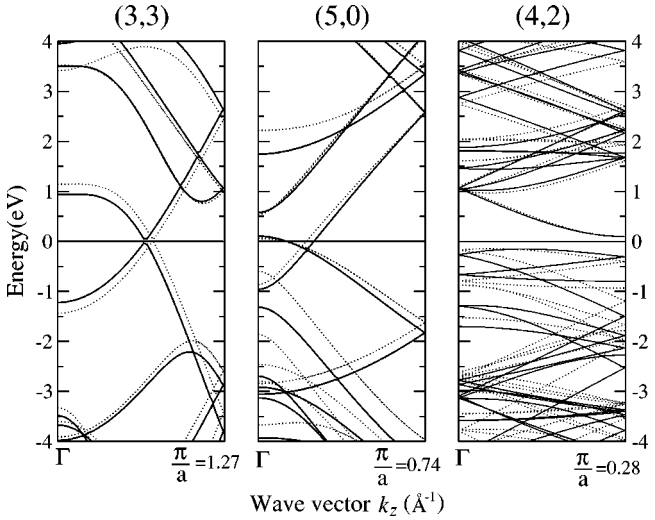

FIG. 5. Solid line represents the calculated electronic band structures of the 4-Å SWNT's with the ideal cylindrical structure. Dotted line represents the same calculation with the relaxed structure. The Fermi level is at 0 eV.

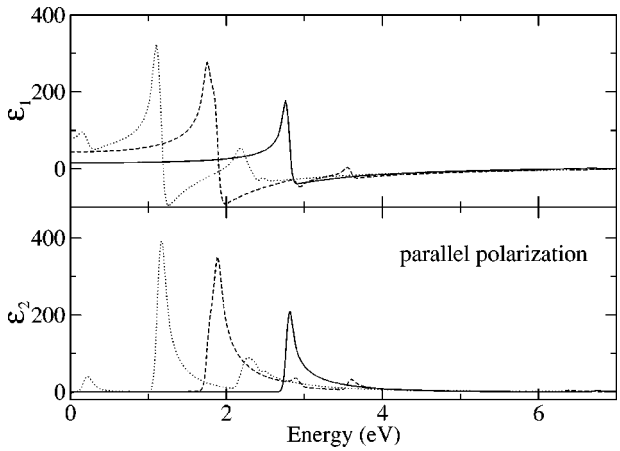

FIG. 6. Calculated dielectric function of the 4-Å-diameter SWNT's for incoming light polarized parallel to the nanotube axis. The upper panel shows the real part and the lower panel shows the imaginary part. The solid line corresponds to the (3,3) armchair tube, the dotted line to the zigzag (5,0), and the dashed line to the chiral (4,2).

SIESTA.[2] The optical matrix elements were calculated including the corrections due to the nonlocality of the pseudopotential.[12] We obtain the imaginary part of the dielectric function ϵ_2, which was then used to calculate the real part ϵ_1 with help of the Kramers-Kronig transformations. The definition of the dielectric function of an isolated nanotube has a certain degree of arbitrariness, since it depends on the concentration of scatterers. In our calculation the density of scatterers is set by the size of the supercell, which does not have a physical meaning. We used the volume of the nanotube V_{NT} to renormalize the calculated dielectric function ϵ_2^{calc} as $\epsilon_2 = (V_{cell}/V_{NT})\epsilon_2^{calc}$, where V_{cell} is the volume of the supercell. Having obtained ϵ_1 and ϵ_2, the other optical properties can be easily calculated.

In Figs. 6 and 7 we show the dielectric function of the

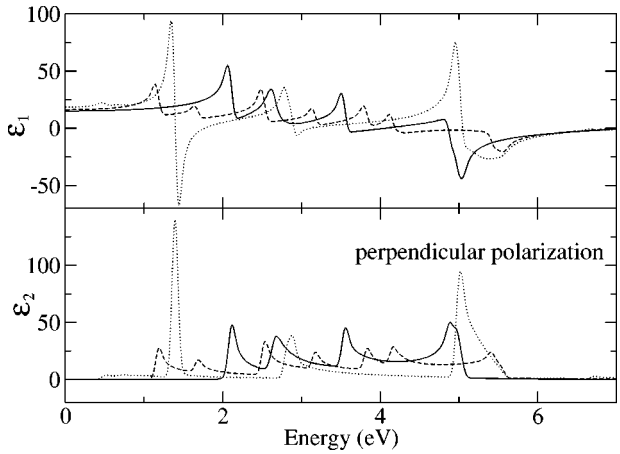

FIG. 7. Calculated dielectric function of the 4-Å-diameter SWNT's for incoming light polarized perpendicular to the nanotube axis. The upper panel shows the real part and the lower the imaginary part. The solid line corresponds to the (3,3) armchair tube, the dotted line to the zigzag (5,0), and the dashed line to the chiral (4,2).

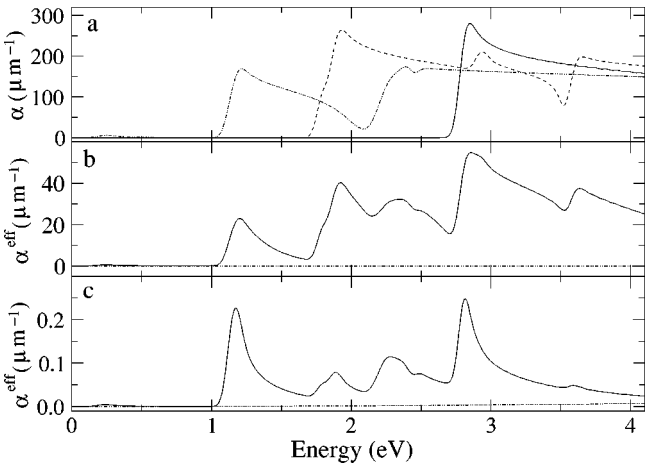

FIG. 8. (a) Optical absorption of the isolated nanotubes under light polarized parallel to the nanotube axis. The solid line corresponds to the (3,3) armchair tube, the dotted line to the zigzag (5,0), and the dashed line to the chiral nanotube (4,2). (b) Solid line represents the effective optical absorption of the zeolite-SWNT composite, assuming the same concentration of (3,3), (5,0), and (4,2) nanotubes. Dotted line represents optical absorption for the zeolite crystal. (c) Solid line represents effective optical absorption of the zeolite-SWNT composite, assuming a ratio of 0.5:0.4:0.1 for the concentration of (5,0), (3,3), and (4,2) nanotubes and a nanotube filling fraction of 2×10^{-4}, which yields a better quantitative agreement with the experimental data. We assumed a sample width of 10 μm (Ref. 1). Dotted line represents optical absorption for the zeolite crystal. In (b) and (c), the optical absorption was corrected for the reflectivity of the sample. However, this correction leaves the results almost unaffected. Note the different scales in the three panels.

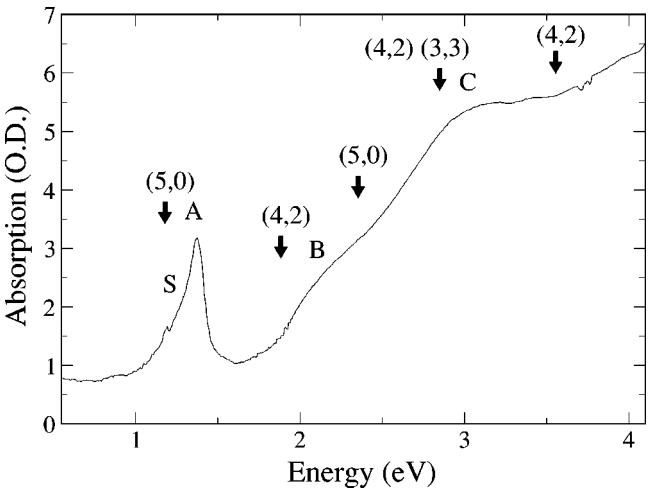

FIG. 9. Optical absorption spectrum of the SWNT-containing zeolite crystal for incident light polarized parallel to the nanotube axis. Taken from Ref. 1. The arrows indicate our assigment of the absorption peaks to individual chiralities.

three SWNT's for the case of light polarized parallel and perpendicular to the nanotube axis, respectively. Due to the anisotropy of the nanotubes, their response in these two configurations is radically different. ϵ_2 gives an idea of the optical absorption. In the parallel configuration, the absorption is concentrated in the 1–3 eV region. Under perpendicularly polarized light, the absorption range extends to 5.5 eV, and the response is at least three times weaker.

Li *et al.*[1] measured polarized absorption spectra for the 4-Å SWNT's arrayed in the one-dimensional channels of a zeolite crystal. They observed a homogeneous decrease in the absorption with increasing polarization angle. This is due to the screening of the electric field perpendicular to the nanotube axis, also known as the depolarization effect,[13] and does not allow the comparison with our results for perpendicular polarization. From this point on, we concentrate on the results under parallel polarized light. In Fig. 8(a), the calculated optical absorption α of the three free-standing SWNT's is shown. For a direct comparison of our results with the experiment, we must include the effect of the zeolite on the optical properties. The van der Waals interaction between nanotube and zeolite has been shown to be very weak[14] (less than 50 meV/atom for the tube sizes considered here), as well as the influence of the zeolite on the electronic structure of the nanotube. We, therefore, neglect this interaction, and treat the zeolite-nanotube composite as a homogeneous material with an effective dielectric constant. This approximation is justified in the long-wavelength limit, which applies in our case. However, it implies that we are neglecting possible depolarization effects in the nanotube due to the zeolite. We calculated an effective dielectric function using the weighted average of the constituents,[15]

$$\epsilon_{\mathrm{eff}}(\omega)=\frac{f[\epsilon_{(3,3)}+\epsilon_{(5,0)}+\epsilon_{(4,2)}]}{3}+(1-f)\epsilon_{\mathrm{zeol}}, \qquad (1)$$

where f, the filling fraction of the nanotubes, is defined as

$$f=\frac{\pi R^2}{a^2\cos 30^\circ}\approx 8\%, \qquad (2)$$

under the assumption that all channels are completely filled. $a=1.37$ nm is the distance between the centers of two adjacent channels in the zeolite crystal and R is the radius of the nanotubes. The concentration of the three different SWNT's was supposed to be homogeneous. We applied Eq. (1) to the imaginary part of the dielectric function neglecting the contribution of the zeolite. This is justified by the measurements of the optical absorption of pure zeolite by Li *et al.*[1] and Hoffmann *et al.*;[16] the latter can be seen in Fig. 8. An effective α was calculated from ϵ_{eff}, the result is shown in Fig. 8(b). The three peaks in α^{eff} correspond well to the experi-

TABLE II. Energies in eV of the experimental and calculated optical absorption maxima of the SWNT containing zeolite. The calculated values are aligned to the corresponding experimental peaks.

Experiment (Ref. 1)	(3,3)	(5,0)	(4,2)
(*S*) 1.2			
(*A*)1.37		1.2	
(*B*) 2.1		(2.4)	1.9
(*C*) 3.1	2.9		3.0–(3.6)

mental results shown in Fig. 9, where the calculated absorption maxima are indicated by arrows. In Table II, the experimental and calculated energies of the absorption maxima are shown; the agreement is excellent. We obtain three peaks equivalent to peaks *A*, *B*, and *C* in the experiment, and are able to identify them as coming mainly from the tubes indicated in Fig. 9. The assignment differs slightly from the one of Li *et al.*,[1] who did not calculate the absorption explicitly. The point group they used did, however, not include the horizontal rotations and thus gave incorrect selection rules [the point group of the (4,2) tube is D_{28} (Ref. 8)]. Contrary to their results, we do not obtain any appreciable absorption due to the (4,2) nanotube below 1.8 eV. The shoulder *S* below the main peak at 1.2 eV does not appear in our calculations. The maximal deviation in the position of the peaks is $\approx 14\%$, which is to be expected from the inaccuracy of local-density (LDA) to describe the energies of excited states, and comparable to the errors of $\approx 10-20\,\%$ reported by Li *et al.*[1] and Reich *et al.*[11]

Since each of the nanotubes gives rise to features in the optical spectrum at different energies, we can use the intensity of the experimental peaks to make a rough estimate of the proportion of nanotubes with each chirality. Although a direct fit of the experimental data with the theoretical spectra is difficult due to uncertainties such as the background in the experimental curves. We found that a proportion of 0.5:0.4:0.1 for the concentration of the (5,0), (3,3), and (4,2) nanotubes optimizes the agreement between the calculations [Fig. 8(c)] and the experiment. The abundance of the chiral (4,2) tubes seems to be lower than of the achiral tubes, a result that supports recent experimental studies indicating a lower concentration of (4,2) nanotubes than of (5,0) and (3,3) tubes.[17] The filling fraction we obtained from the experimental data, 2×10^{-4}, is two orders of magnitude smaller than expected from the volume of the zeolite channels, see Eq. (2). Partly, this difference might be due to the experimental setup, e.g., the non-normal incidence of the light in a microscope setup.[1] Nevertheless, our finding also indicates that only a part of the zeolite channels is filled with nanotubes.

In summary, we performed LDA calculations of the geometry, band structure, and the optical properties of (3,3), (5,0), and (4,2) SWNT's. We found significant deviations from the ideal cylindrical structure. The accuracy of our calculations of the electronic band structure was tested by comparing with plane-wave calculations of graphene, obtaining a very good agreement between both computational schemes. We found the (5,0) nanotube to be metallic in contrast to the prediction of the zone folding approximation and explained this feature as an effect of the strong curvature of the nanotube walls. A strong anisotropy of the optical response was found, as shown in the calculated complex dielectric function of the nanotubes. The optical absorption under parallel polarized light was compared with measurements on zeolite-grown nanotubes. An effective optical absorption coefficient was calculated and used to successfully interpret the experiments of Li *et al.*[1]

We thank J. Maultzsch for helpful discussions. We acknowledge the Ministerio de Ciencia y Tecnología (Spain) and the DAAD (Germany) for a Spanish-German Research action (Grant No. HA 1999-0118). D.S.P. acknowledges support from the Spanish MCyT and CSIC under the ''Ramón y Cajal'' program. P.O. acknowledges support from Fundación Ramón Areces (Spain), EU Project No. SATURN IST-1999-10593, and Spain-DGI Project No. BMF2000-1312-002-01.

[1] Z.M. Li, Z.K. Tang, H.J. Liu, N. Wang, C.T. Chan, R. Saito, S. Okada, G.D. Li, J.S. Chen, N. Nagasawa, and S. Tsuda, Phys. Rev. Lett. **87**, 127401 (2001).

[2] J.M. Soler, E. Artacho, J.D. Gale, A. García, J. Junquera, P. Ordejón, and D. Sánchez-Portal, J. Phys.: Condens. Matter **14**, 2745 (2002).

[3] D. Sánchez-Portal, P. Ordejón, E. Artacho, and J.M. Soler, Int. J. Quantum Chem. **65**, 453 (1997).

[4] J.P. Perdew and A. Zunger, Phys. Rev. B **23**, 5048 (1981).

[5] N. Troullier and J.L. Martins, Phys. Rev. B **43**, 1993 (1991).

[6] J. Junquera, O. Paz, D. Sánchez-Portal, and E. Artacho, Phys. Rev. B **64**, 235111 (2001).

[7] E. Artacho, D. Sánchez-Portal, P. Ordejón, A. García, and J. Soler, Phys. Status Solidi B **215**, 809 (1999).

[8] M. Damnjanović, I. Milošević, T. Vuković, and R. Sredanović, Phys. Rev. B **60**, 2728 (1999).

[9] D. Sánchez-Portal, E. Artacho, J. Soler, A. Rubio, and P. Ordejón, Phys. Rev. B **59**, 12 678 (1999).

[10] X. Blase, L.X. Benedict, E.L. Shirley, and S.G. Louie, Phys. Rev. Lett. **72**, 1878 (1994).

[11] S. Reich, C. Thomsen, and P. Ordejon, Phys. Rev. B **65**, 155411 (2002).

[12] A.J. Read and R.J. Needs, Phys. Rev. B **44**, 13 071 (1991).

[13] L.X. Benedict, S.G. Louie, and M.L. Cohen, Phys. Rev. B **52**, 8541 (1995).

[14] O. Dubay and G. Kresse, in *Proceedings of the International Winterschool on Electronic Properties of Novel Materials, Kirchberg, 2002*, edited by H. Kuzmany, J. Fink, M. Mehring, and S. Roth (AIP, Melville, N.Y., 2002).

[15] J.M. Pitarke and F.J. García-Vidal, Phys. Rev. B **63**, 073404 (2001).

[16] K. Hoffmann, F. Marlow, and J. Caro, Zeolites **16**, 281 (1997).

[17] Z.K. Tang (private communication).